Focal gamma activity in frontal cognitive control regions revealed using intraoperative electrocorticography

Moataz Assem[1*], Michael G. Hart[2], Pedro Coelho[3], Rafael Romero-Garcia[4], Alexa McDonald[5], Emma Woodberry[5], Robert C. Morris[2], Stephen J. Price[6], John Suckling[4,7,8], Thomas Santarius[2,6,9], John Duncan[1,10], Yaara Erez[11,1*]

1 Medical Research Council, Cognition and Brain Sciences Unit, University of Cambridge
2 Department of Neurosurgery, Cambridge University Hospitals NHS Foundation Trust
3 Neurophys Limited
4 Department of Psychiatry, University of Cambridge
5 Department of Neuropsychology, Cambridge University Hospitals NHS Foundation Trust
6 Division of Neurosurgery, Department of Clinical Neurosciences, University of Cambridge.
7 Behavioural and Clinical Neuroscience Institute, University of Cambridge
8 Cambridge and Peterborough NHS Foundation Trust
9 Department of Physiology, Development and Neuroscience, University of Cambridge
10 Department of Experimental Psychology, University of Oxford
11 Faculty of Engineering, Bar-Ilan University, Ramat-Gan, Israel

*Corresponding authors:

Moataz.assem@mrc-cbu.cam.ac.uk

Yaara.Erez@biu.ac.il

Abstract

How the frontal lobe is organized to control cognition remains puzzling. Functional MRI (fMRI) studies relate cognitive control to localized frontal patches, part of a brain-wide fronto-parietal network (FPN). However, this functional organization remains unverified using direct electrophysiological recordings. Here, we placed electrodes on the lateral frontal cortex in patients undergoing awake craniotomy for tumour resection. Patients performed verbal tasks with a manipulation of attentional switching, a canonical executive demand. Comparing high versus low demands revealed circumscribed frontal regions with power increases in the gamma range (30-250 Hz). This contrasted with spatially distributed power decreases in the beta range (12-30 Hz). Further, electrodes showing significant gamma power increases were more likely to occur within a canonical fMRI-defined FPN and showed stronger gamma power increases compared to electrodes outside the FPN, even at the single patient level. Thus, using similar task manipulations, ECoG and fMRI signals converge on delineating specific regions of lateral frontal cortex linked to cognitive control.

Introduction

The anatomical and functional organization of the human frontal lobe remains a puzzling problem. Functional MRI (fMRI) studies consistently reveal circumscribed frontal regions that co-activate in association with multiple cognitive control demands (Assem et al., 2020; Cole et al., 2016; Corbetta and Shulman, 2002; Erez and Duncan, 2015; Fedorenko et al., 2013; Jackson et al., 2016; Muhle-Karbe et al., 2014; Shashidhara et al., 2020, 2019) and form part of the wider functionally integrated fronto-parietal network (FPN) (Assem et al., 2020; Power et al., 2011; Thomas Yeo et al., 2011). Much uncertainty remains, however, over localisation of cognitive control frontal regions using fMRI on its own because the neuronal origins of its signals are not well understood (Logothetis, 2008). Localization of specific FPN regions remains unverified using electrophysiological data owing to the limited spatial resolution of non-invasive methods such as electro/magneto-encephalography (EEG/MEG) (Farahibozorg et al., 2018).

Here we turned to electrocorticography (ECoG), placing electrodes directly on the frontal cortical surface. ECoG offers high spatial resolution access to local field potentials (LFPs) in the gamma frequency range (30-250 Hz), a well-established index of local cortical processing that cannot be detected with non-invasive methods (Crone et al., 2006; Lachaux et al., 2012). In cognitive control studies, power increases in the gamma range have been linked to heightened attentive states (Bouyer et al., 1981), processing of attended stimuli (Fries, 2001; Helfrich and Knight, 2016; Ray et al., 2008; Szczepanski et al., 2014), working memory, (Haller et al., 2018; Howard, 2003; Mainy et al., 2007) and responses to abstract rules (Voytek et al., 2015). A common limitation for the above-mentioned studies is their lack of anatomical specificity of gamma activity, mostly allocating it to broad labels such as “dorsolateral prefrontal cortex”. Such association cortices are rich in functionally heterogeneous regions (Glasser et al., 2016; Gordon et al., 2016; Yeo et al., 2015, 2011), making it difficult to interpret findings across studies and relate them to non-invasive brain imaging data.

In this study, we used ECoG during awake brain surgeries from 13 patients while they performed two tasks with a varying level of control demand: simple counting (1 to 20; count) and switching between counting and reciting the alphabet

(1, a, 2, b, 3, c, up to 20; switch) (**Figure 1; see Methods**). Following a previous demonstration of the feasibility of ECoG for cognitive control mapping (Erez et al., 2021), here we use dense coverage of the frontal cortex to characterize the power modulations associated with increased cognitive demand, and importantly, directly link them to the FPN. Many similar control demand manipulations in fMRI studies have consistently revealed localized frontal control co-activations (Fedorenko et al., 2013; Hugdahl et al., 2015). Together with the established links between fMRI responses with increased gamma power (Logothetis et al., 2001; Mukamel et al., 2005; Siero et al., 2013) as well as gamma increases across cognitive control tasks (Crone et al., 2006; Lachaux et al., 2012), we predicted that increased cognitive demand will be accompanied by gamma power increases, especially within the FPN. We further predicted that gamma increases will be accompanied by power decreases in the beta range (12-30 Hz), based on previous findings that link opposing power modulations in these frequency bands (Crone et al., 2006; Hermes et al., 2012b; Podvalny et al., 2015).

Results

Switch>count contrast reveals local increases in gamma power contrasting with widespread decreases in beta power

Across 59 electrodes (**Figure 1c**), we first examined spectral power changes for the switch>count contrast for three classical frequency bands: high gamma (HG, 70-250 Hz), low gamma (LG, 30-70 Hz) and beta (12-30 Hz). In this contrast, positive values indicate power increases in switch compared to count, while negative values indicate power decreases. For the HG and LG bands, electrodes with significant power modulations showed predominantly increases (**Figure 2),** and all but one of the electrodes that showed significant LG increases also showed HG increases. In contrast, changes in the beta band showed predominantly power decreases (**Figure 2).** There was only partial overlap between locations of electrodes showing gamma increases and beta decreases (for HG, r=0.54, p<0.0001; for LG, r=0.32, p=0.003). Importantly, gamma power increases were spatially circumscribed, while beta

decreases were more broadly distributed across the recording area. To quantify this observation, we compared the Euclidean distances between all pairs of electrodes with significant power changes for each of the three bands. We found that distances between significant electrodes for the HG and LG bands were smaller than for the beta band (unpaired t-test; HG>beta: t_{877}=-7.8, p=1.5x10^{-14}; LG>beta: t_{604}=-2.2, p=0.03; repeated unpaired t-test after excluding electrodes lying on the motor cortex: HG>beta: t_{784}=-3.5, p=0.0005; LG>beta: t_{511}=-0.98, p=0.33). Although this measure is, at least in part, affected by the spatial distribution of the electrodes, it nevertheless captures that, along the lateral frontal cortex, increased cognitive demand is associated with a localized increase in LFPs' high frequency band power and a spatially distributed decrease in low frequency power.

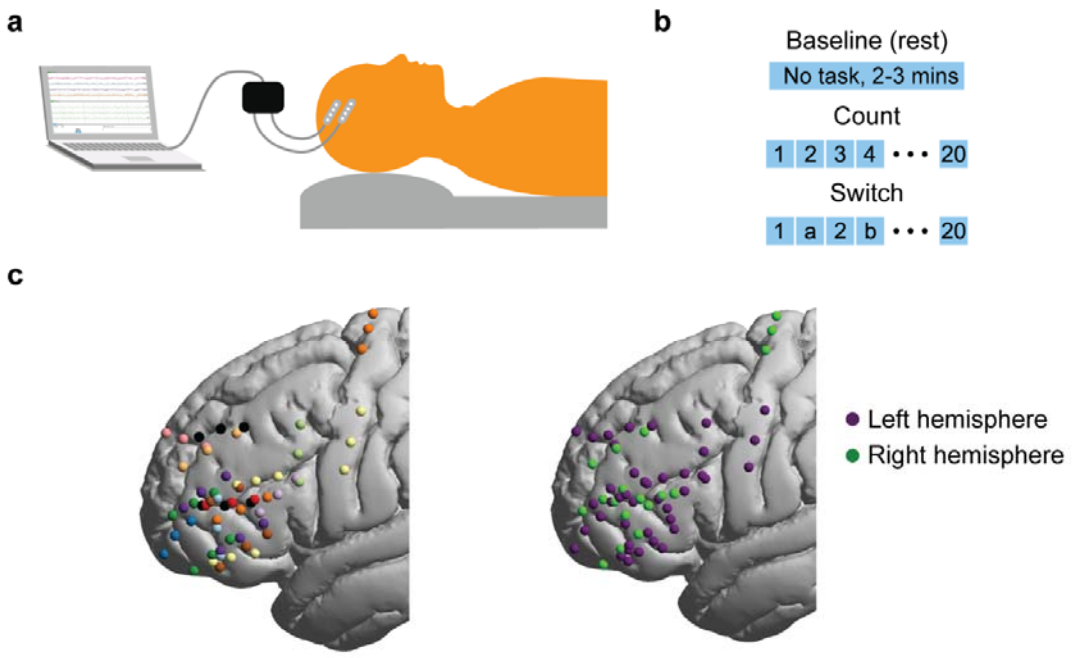

Figure 1. Intraoperative ECoG setup and electrode localization. (a) Intraoperative setup: Patient is awake during the three experimental conditions and the electrophysiological signals are simultaneously recorded using electrode strips placed directly on the cortical surface. (b) Experimental conditions: one rest (no task) and two verbal tasks. The count task involved simple counting from 1 to 20. The switch task involved alternating between numbers and letters. (c) *Left*: Electrode distribution for each patient in a separate color (13 patients, 59 electrodes after bipolar re-referencing). Electrodes from both hemispheres projected onto the left. *Right*: hemispheric distribution of electrodes.

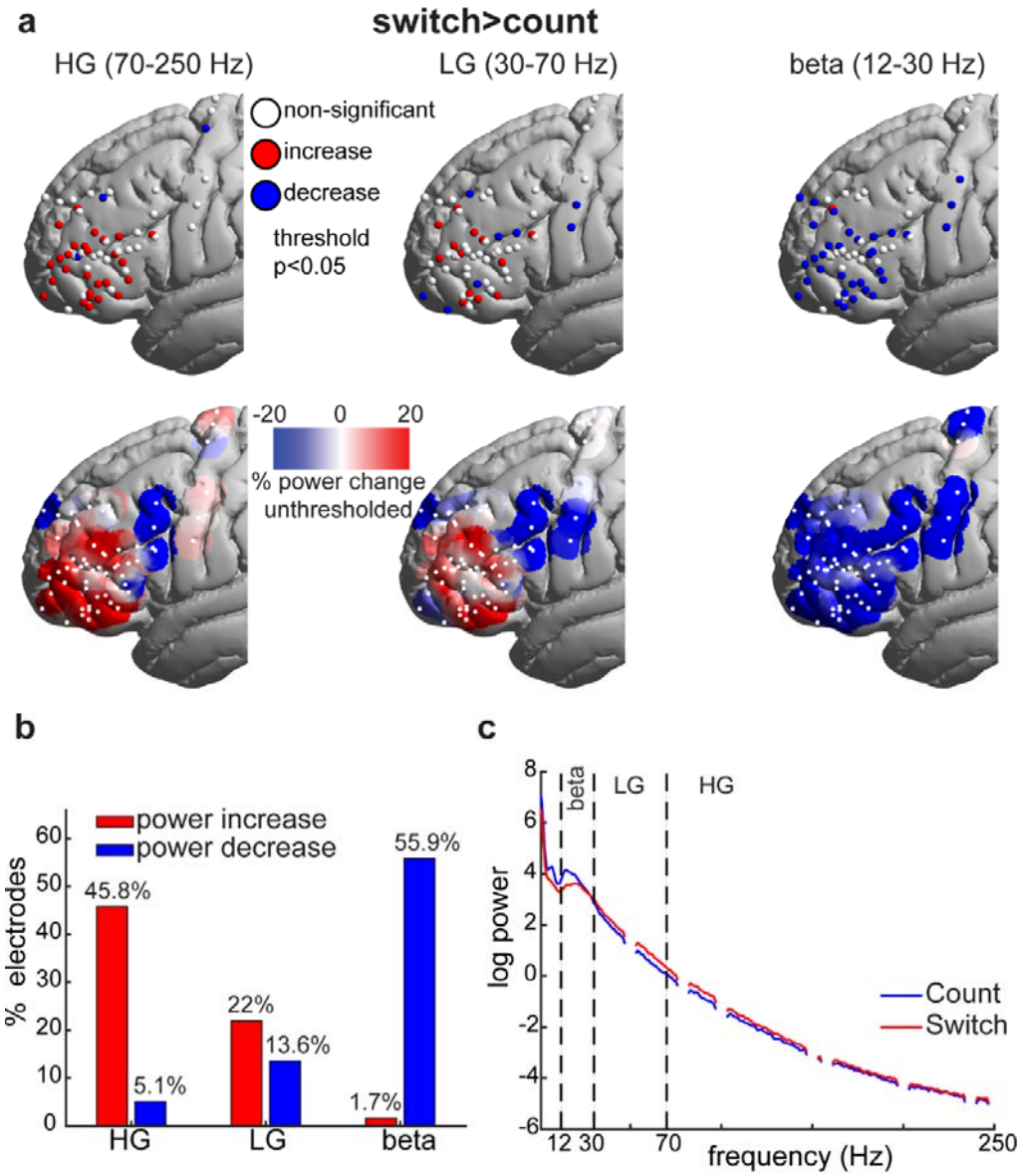

Figure 2. Switch>count spectral power modulations. (a) *Top*: Electrodes with significant (thresholded at $p<0.05$, uncorrected) power increases (red), decreases (blue) and non-significant changes (white). *Bottom*: Unthresholded average smoothed data. Power for each electrode (white dots; including electrodes with non-significant power changes) was spatially smoothed such that the value at each surface vertex is the average of the overlapping powers within a sphere of a 10 mm radius. (b) Proportion of electrodes (out of a total of 59) showing significant power modulations for each of the frequency bands. (c) Average of PSDs of all electrodes showing significant changes in all three bands: HG and LG power increases as well as beta power decreases. Notch filtered noise frequency bands (see methods) are hidden.

High frequency power increases overlap with the fMRI-defined FPN

Next we tested whether electrodes showing gamma increases would overlap with a canonical mask of the cognitive control FPN as defined in independent fMRI data (**see Methods**). 33 electrodes were located within the FPN, while 26 were outside this network (**Figure 3a)**. Of the FPN electrodes, 61.3% showed a significant HG increase in the switch>count contrast, compared to 28.6% of non-FPN electrodes (**Figure 3b**). LG increases showed a similar trend (29% vs. 14.3%). In contrast, the proportions of electrodes showing beta power decreases were similar for FPN and non-FPN (51.6% vs. 60.7%). Indicating the specificity of the findings to frontal electrodes, all findings replicated after excluding the motor electrodes (HG: 61.3% vs. 36.4%; LG: 29% vs. 18.2%; Beta: 51.6% vs. 63.6%). Therefore, only gamma increases, but not beta decreases, were more likely within the FPN compared to outside the network.

In a subsequent analysis, we examined data across all electrodes, irrespective of significant changes in individual electrodes. Here too, HG and LG power increases were significantly stronger in FPN than in non-FPN electrodes **(Figure 3c;** unpaired t-test, HG: t_{57}=2.66, p=0.005; LG: t_{57}=2.71, p=0.004, p-values are one-tailed due to our directional prediction of gamma increases within the FPN). Again, there was no significant difference between FPN and non-FPN electrodes for beta power decreases (t_{57}=1.2, p=0.2, two-tailed as we had no specific directional prediction). Similarly, all findings replicated after excluding the motor electrodes (HG: t_{51}=2.6, p=0.006; LG: t_{51}=2.5, p=0.008; one-tailed; beta: t_{51}=1.01, p=0.3; two-tailed).

A limitation of the previous analyses is that most effects could be driven by a subset of patients. To address this, we used data from all the patients who each had electrodes overlapping with both FPN and non-FPN regions to perform a within-subject analysis (11 out of the 13 patients). The results showed that within the same patient, FPN electrodes showed statistically larger LG power compared to non-FPN electrodes (Wilcoxon signed-rank test; p=0.02, one-tailed) and no differences (though trending) for the beta power (p=0.08, two-tailed). Here, however, differences for HG were not significant (p=0.2, one-tailed). These results hold even

after excluding the apparent outlier patient in **Figure 3d (**HG: p=0.2; LG: p=0.01; both one-tailed; beta: p=0.049, two-tailed) and after excluding the motor electrodes (HG: p=0.2; LG: p=0.02; both one-tailed; beta: p=0.3, two-tailed)

Collectively, these results suggest that demand-related power increases in the gamma band co-localize with the fMRI-identified FPN. Thus, results from two different modalities (ECoG and fMRI) converge in defining a localized region within the lateral frontal lobe related to cognitive control.

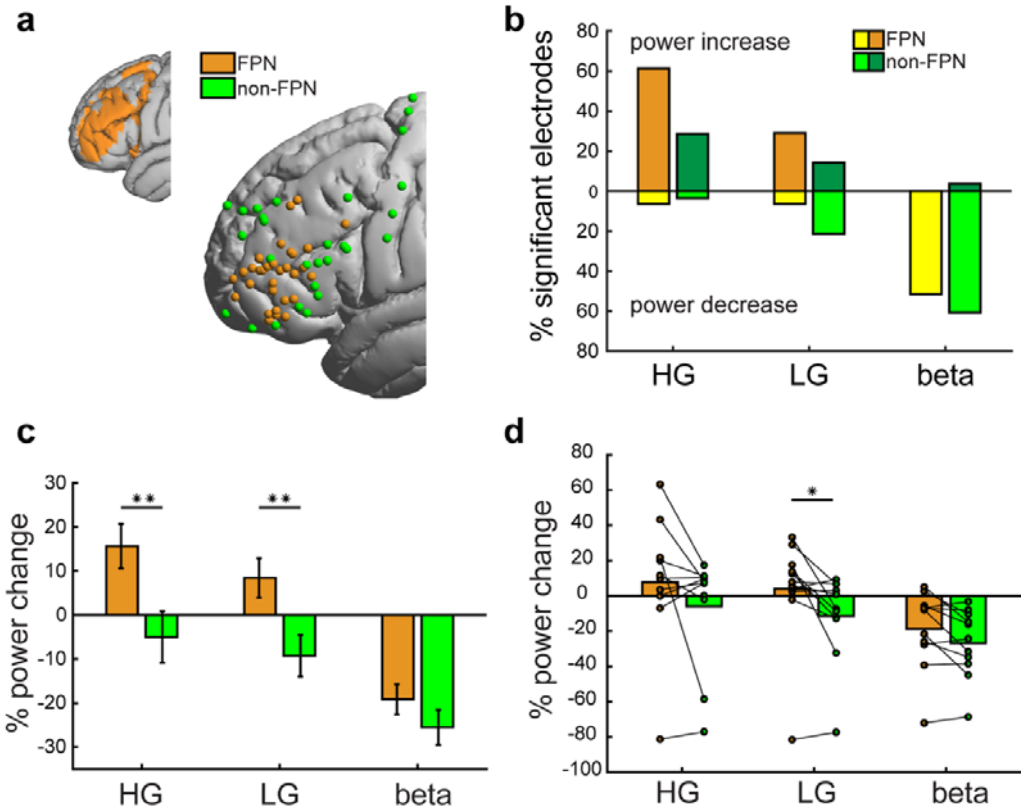

Figure 3. Switch>count broadband gamma power increases overlap with FPN. (a) Electrodes coloured based on their overlap with the canonical fMRI FPN mask in volume space. *Top left inset*: A cortical surface visualization of the volumetric canonical fMRI FPN mask (Thomas Yeo et al., 2011) (Note: this is for illustrative purposes only and may include slight distortions resulting from volume-to-surface transformation). (b) Percentage of electrodes showing significant power modulations out of all electrodes located within (orange and yellow) and outside (dark and light green) the FPN. Darker coloured bars (above the zero line) show percentage of electrodes with power increases. Lighter coloured bars (below the zero line) show percentage of electrodes with power decreases. (c) Power modulations of all electrodes within and outside the FPN for each frequency band. **p<0.01, one-tailed, unpaired t-test. (d) A within-subjects comparison of power changes between FPN and non-FPN electrodes. Each dot represents average power across each group of electrodes for one patient. *p<0.05, for one-tailed tests, Wilcoxon signed-rank test.

Power modulations in the count>rest contrast

Next we sought to assess whether the localized gamma increases, identified in the switch>count contrast where the conditions are matched on multiple aspects (e.g. speech, counting), would also replicate in the count>rest contrast where those aspects are not matched. For each frequency band, and for each electrode, we calculated the change in power for switch>count and count>rest. The two were uncorrelated across electrodes for gamma (HG: r=-0.07, p=0.53; LG: r=-0.09, p=0.42), with a weak correlation for beta (r=0.22, p=0.045), indicating different topographical arrangement for modulations in the two contrasts (**Figure 4a**).

Further, the percentage of electrodes with significant gamma increases was similar between FPN and non-FPN electrodes (**Figure 4b,** HG: 32.3% vs. 39.3%; LG: 22.6% vs. 17.9%). Neither the average power modulations across electrodes (**Figure 4c;** unpaired t-test, HG: t_{57}=-1.28, p=0.90; LG: t_{57}=-0.67, p=0.78, one-tailed; beta t_{57}=-0.69, p=0.49, two-tailed) nor the within-subject analysis (**Figure 4d;** Wilcoxon signed-rank test, HG: p=0.86, LG: p=0.58, one-tailed for both; beta: p=0.52, two-tailed) showed any significant differences between FPN and non-FPN electrodes across the three bands. Again, these results were stable after excluding the apparent outlier patient in **Figure 4d** (within-subject analysis: Wilcoxon signed-rank test, HG: p=0.99*; LG:* p=0.75, one-tailed for both; beta: p=0.77, two-tailed)**.**

Interestingly, count>rest gamma increases were shifted posteriorly to switch>count increases (**Figure 4e**). To quantify this, we compared y-coordinates (anterior-posterior axis) of electrodes showing significant gamma increases between switch>count and count>rest contrasts. The results confirmed a posterior shift for the electrodes with significant HG increases in the count>rest contrast (Wilcoxon signed-rank test, HG: p=0.02, LG: p=0.07). Altogether, these results demonstrate that the well-controlled switch>count contrast is most suitable for localizing cognitive control-related frontal regions using gamma power modulations.

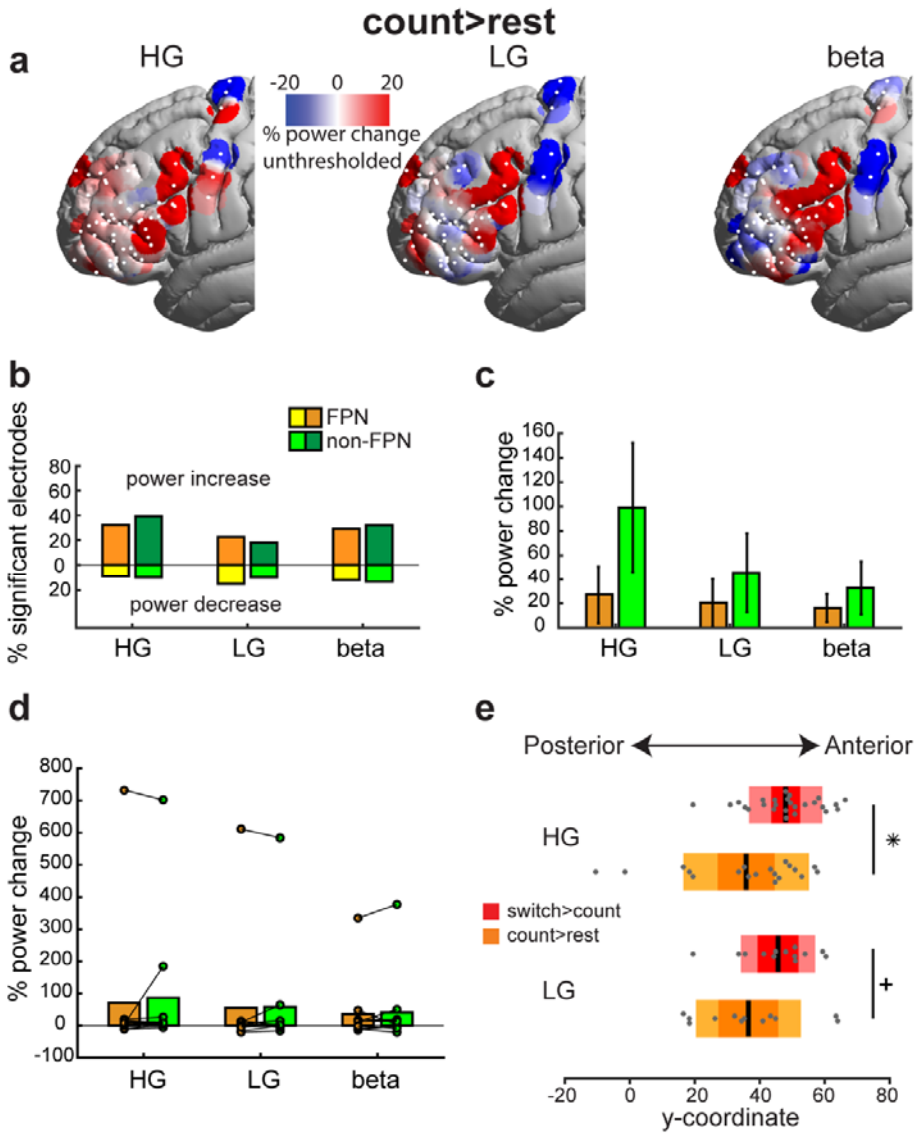

Figure 4. Power modulations for the count>rest contrast. (a) Surface projection of power modulations for the count>rest contrast. Remaining details are identical to **Figure 2a.** (b-d) Comparison of count>rest power changes between FPN and non-FPN electrodes. Details are identical to **Figure 3(b-d).** (e) Box plots of y-coordinate of electrodes with significant power increases. Middle black line: mean; darker box limits: 1 SD; lighter box limits: 95% CI. *p<0.05 +p=0.07, using Wilcoxon rank sum test.

Discussion

We recorded LFP signals using ECoG from the lateral frontal surface of human patients undergoing awake craniotomies for tumour resections. The results revealed a circumscribed frontal region that shows increases in broadband gamma power with increased task demands. Localized gamma increases were accompanied by spatially broad beta power decreases. Electrodes showing gamma increases overlapped with a canonical mask of the fMRI-defined FPN. Thus, ECoG and fMRI converge on fine-scale functional differentiation within the human frontal lobe, delineating specific frontal regions associated with cognitive control.

Some evidence from previous electrophysiology studies suggests that gamma power increases in frontal regions are associated with executive processes such as attention, working memory and abstract rule use (Fries, 2001; Helfrich and Knight, 2016; Ray et al., 2008; Szczepanski et al., 2014). However, invasive human studies have rarely systematically assessed the anatomical distribution of gamma increases, with most studies reporting isolated findings in individual electrodes or coarse-scale anatomical distinctions (Helfrich and Knight, 2016; Lachaux et al., 2012). This lack of detailed topographical assessment limits our ability to relate findings across studies and across neuroimaging modalities. Our findings represent a significant advance over previous ECoG studies, demonstrating that a circumscribed region along the lateral frontal surface robustly shows increases in gamma power during an executive task, further extending our knowledge about the electrophysiological properties of the FPN. Although some previous studies have reported different reliabilities and putative physiological origins for HG and LG (Buzsáki and Wang, 2012; Crone et al., 2006; Lachaux et al., 2012; Ray and Maunsell, 2011), in our data both gamma bands were broadly in agreement.

Our results suggest converging evidence from ECoG and fMRI modalities for control-related parcellation of the lateral frontal cortex. We used a task demand manipulation similar to one that was previously shown to recruit control regions in fMRI studies (Assem et al., 2020; Fedorenko et al., 2013; Shashidhara et al., 2020) and the observed gamma power increases associated with increased demand co-localized with a canonical FPN derived from independent resting-state fMRI data from healthy participants. Previous studies have linked localized gamma increases

with corresponding fMRI activations in early cortical regions (Engell et al., 2012; Hermes et al., 2012a; Nir et al., 2007). Accordingly, gamma increases were generally interpreted to reflect localized task-related processing. The current results extend these reports to the domain of cognitive control in frontal regions.

In contrast to focal increases in the gamma range, we observed spatially broad decreases in power in the beta band (and other lower frequencies) which were not confined to the FPN. It has been previously shown that synchronization in lower frequency bands between fronto-parietal regions increased during executive tasks e.g. (Voytek et al., 2015). Our findings suggest that increases in beta synchrony may be accompanied by decreases in power. Concerning the relation between gamma increases and beta decreases, one suggestion is that these reflect two sides of the same process, a rotated power spectrum around a middle range frequency (Helfrich and Knight, 2016; Podvalny et al., 2015). Recent evidence, however, argues against this simple interpretation, showing that depending on the cortical region, increases in high gamma power are not necessarily accompanied by decreases in low frequency power (Fellner et al., 2019). In line with this, the current results also showed that beta decreases were more spatially broad and were not necessarily accompanied by gamma increases. Another framework proposes a hybrid spiking-synaptic plasticity working memory model, in which bursts of spikes (gamma increases) in superficial layers serve to encode and maintain working memory content, while beta, which is assumed to have an inhibitory role, is suppressed in deeper layers to allow superficial gamma bursts (Lundqvist et al., 2011; Miller et al., 2018). This model is specific for regions that are involved in working memory processes. As it stands, however, this model may need extension to explain beta power decreases within but also outside of FPN.

Our careful anatomical analysis has additionally revealed a posterior shift of gamma increases in count>rest compared to the switch>count contrast. One possibility is that this shift mirrors fMRI studies showing an anterior-posterior cognitive demand gradient across the lateral frontal surface, with easier tasks involving more posterior regions and more challenging tasks recruiting more anterior regions (Assem et al., 2020; Badre and Nee, 2018; Shashidhara et al., 2019). Another possibility is related to the conditions that comprise the two contrasts. While the switch>count contrast compared conditions that are closely matched on features such as speech and counting task, the count>rest contrast is less

controlled. Accordingly, changes in activity may be related to several differences between the conditions, most prominently speech production (the count condition includes speech while the patient remains silent during the rest condition). Plausibly, posterior gamma increases might also reflect articulation or language related processing in the posterior inferior frontal gyrus (Basilakos et al., 2018).

Finally, our findings open the door for extending clinical functional mapping to the domain of cognitive control during tumour resection surgeries (Erez et al., 2021; Hart et al., 2020). The link of increased gamma power to the FPN establishes a critical anatomo-functional foundation for this approach. Matching the fine scale of regional specializations within frontal cortex, our results suggest that distinct functional regions may be practically mapped in the context of awake tumor surgery.

Methods

Patient recruitment

Twenty-one patients were recruited. Patients were recruited from the pool of patients with glioma who have been indicated to undergo awake craniotomy for the resection of the tumour at the Department of Neurosurgery at Cambridge University Addenbrooke's Hospital (Cambridge, UK). Data from thirteen patients were complete and were included in the study (age range 22-56; 6 males; see **Table 1** for patient demographics). Data from the remaining eight patients were excluded either due to technical difficulties (n=6; e.g. inability to localize electrodes correctly during the surgical theatre) or an inability to perform the tasks during the surgery (n=2). All study procedures were approved by the East of England - Cambridge Central Research Ethics Committee (REC reference 16/EE/0151). All patients gave written informed consent to participate and were aware that the research would not benefit themselves, or impact their clinical care before, during or after surgery.

Experimental procedures

The patients were familiarized with the tasks during standard pre-operative clinic visits and as part of a pre-operative research-dedicated assessment. During the surgery and following the craniotomy, EEG (electroencephalogram) was recorded from scalp electrodes C3, C4 and Cz referenced to Fz for the purposes of monitoring anaesthetic depth and stimulation-related seizure activity. When the sedation was stopped the EEG evolved from high voltage, semi-rhythmic alpha and theta range components to a continuous trace consisting of the faster beta range frequencies (>13Hz) and low voltage activities in all derivations until the patients were awake. These low voltage beta range rhythms (normal awake activity) persisted during wakefulness and only then did cognitive testing commence. In all patients, testing was performed prior to tumour resection, except for one patient, where testing was performed after partial resection due to clinical considerations. **Figures 1a,b** illustrate the intraoperative setup and cognitive tasks. During testing, all personnel in the surgical theatre were asked to limit their conversations to

minimize disruptions. Patients performed one baseline task and two cognitive tasks. For the baseline task, the patients were asked to stay calm and remain silent for a period of 2-3 minutes (rest). The two cognitive tasks were simple counting (1 to 20; count) and alternate between counting and reciting the alphabet (1, a, 2, b, 3, c, up to 20; switch). Each task condition was repeated for 2-5 trials (median for both = 4 trials) based on each patient's ability and time constraints during the surgery. Trial onset and offset markers were manually recorded on the acquisition system. Trial durations were 20.1±7.4s and 29.4±9.4s for the count and switch conditions, respectively. Most patients were instructed to alternate between trials of the count and switch conditions, though on a few occasions some trials of the same condition were performed in succession. Only correctly performed trials (i.e., no errors in simple or alternate counting) were included in the analysis (e.g., a failed switch trial that was excluded: 1, a, 2, b, 3, b, 4, b, 5, b, 6, b…).

MRI acquisition

MRI data were acquired pre-operatively using a Siemens Magnetom Prisma-fit 3 Tesla MRI scanner and 16-channel receive-only head coil (Siemens AG, Erlangen, Germany). Structural anatomic images were acquired using a T1-weighted (T1w) MPRAGE sequence (FOV = 256 mm x 240 mm x 176 mm; voxel size = 1 mm isotropic; repetition time (TR) = 2300 ms; echo time (TE) = 2.98 ms; flip angle = 9 degrees).

Electrode localization

The extent of craniotomy of all patients was determined by clinical considerations to allow for tumour resection. Based on the craniotomy size and location, one to three electrode strips were placed on the cortical surface in regions judged by the neurosurgeon to be healthy (i.e. macroscopically not containing tumour). Strips placed on the tumour or outside of the frontal and motor cortices were excluded from analysis. Each strip was composed of four electrodes. Two types of strips were used with electrode diameter either 5 mm (MS04R-IP10X-0JH, Ad-Tech, Medical Instruments corporation, WI, USA) or 3 mm (CORTAC 2111-04-081, PMT

Corporation, MN, USA). For both strip types, electrode spacing was 10 mm centre to centre.

Electrode locations were determined either using (1) an automated method with a probe linked to a stereotactic neuronavigation system (StealthStation® S7® System, Medtronic, Inc, 24 Louisville, CO, USA) or (2) a semi-manual grid method using intraoperative photographs and a grid-like delineation of cortical sulci and gyri. Most electrodes (51/79) were localized using the automated method, and due to occasional technical limitations, 28 electrodes were localized using the grid method. Both methods are detailed below.

(1) Stereotactic neuronavigation: A hand-held probe was placed at the centre of each electrode, automatically registering its physical coordinates, using the neuronavigation system, to the patient's native high resolution preoperative T1w scan. In some cases, coordinate data were available for only two or three out of the four electrodes in each strip. This was due to either time constraints during the surgery or because an electrode was located underneath the skull, excluding probe placement. Each patient's native T1w scan was linearly co-registered with the MNI template volume at 2 mm resolution using FLIRT as implemented in FSL (Jenkinson et al., 2012) using 12 degrees of freedom (full set affine transformation) and the correlation ratio cost function. The resulting native-to-MNI transformation matrix was then used to convert native electrode coordinates to MNI coordinates.

(2) The grid method: This follows the method described in (Havas et al., 2015) and (Ojemann et al., 1989). (a) Visible major sulci were delineated on the intraoperative photographs: precentral sulcus, sylvian fissure, inferior and superior frontal sulci. Spaces between these sulci were populated by vertical lines (1.5 cm apart) to create a grid-like structure. (b) A grid was created in the same way on a template cortical reconstruction of the MNI volumetric map (reconstructed using the HCP structural preprocessing pipeline 4.0.0; https://github.com/Washington-University/HCPpipelines). (c) MNI coordinates for each electrode were extracted by manually marking its approximate location on the template cortical grid while visualized using the Connectome Workbench v1.4.2 (https://www.humanconnectome.org/software/get-connectome-workbench). As the template cortical reconstruction is co-registered with its MNI volumetric version, it facilitated the automatic transformation of any point marked on the surface back to its MNI volumetric coordinates.

For both localization methods, electrode displacements due to brain shifts following the craniotomy were compensated for by back-projecting the electrode locations onto the cortical surface along the local norm vector (Hermes et al., 2010) as implemented in the fieldtrip (v20160629) protocol for human intracranial data (Stolk et al., 2018).

Electrophysiological data acquisition and analysis

Data were recorded using a 32-channel amplifier (Medtronic Xomed, Jacksonville, FS, USA) sampled at 10 KHz. Potential sources of electrical noise such as the surgical microscope, patient warming blanket, and IV pumps were identified and repositioned to avoid signal contamination. The data were recorded via dedicated channels on the acquisition system and two Butterworth online filters were applied: a high-pass filter at 1 Hz and a low-pass filter at 1500 Hz. A ground needle electrode was connected to the deltoid muscle and the electrodes were referenced to a mid-frontal (Fz) spiral scalp EEG electrode.

Data were analyzed offline using EEGLAB (v13.6.5b) and custom MATLAB scripts. The data were downsampled to 2 kHz then re-referenced using a bipolar scheme to detect any activity changes with the highest spatial resolution as well as to avoid contamination of high frequency signals by scalp muscle artefacts detected by the Fz electrode. The last electrode on the strip was excluded from analysis; i.e. for a four-electrode strip, electrode pairs 1-2, 2-3 and 3-4 were used and assigned to electrode positions 1, 2 and 3, respectively. The location of electrode 4 was discarded. Thus, out of the original 79 electrodes, re-referenced data from 59 were used for further analysis (**Figure 1c**). Out of these 59 electrodes, 41 were on the left hemisphere and 18 on the right. 25 electrodes were placed on the middle frontal gyrus (MFG), 28 on the inferior frontal gyrus (IFG) and 6 on motor cortex.

A notch filter was applied at 50 Hz and its harmonics to remove line noise. Notch filtering was also applied at 79 Hz and its harmonics to remove additional noise observed in the data, likely due to equipment in the surgical theatre. Data were then bandpass filtered into 3 classical frequency bands (beta: 12-30 Hz, low gamma (LG): 30-70 Hz, high gamma (HG): 70-250 Hz). Instantaneous power of the timeseries was obtained by squaring the absolute amplitude envelope of the Hilbert transformed data.

The power timeseries data were then segmented into separate conditions and trials. Because trial onset and offset markers were manually recorded, 2s from the beginning and end of the rest trial and 1s from each task trial were excluded to account for human reaction time related error. For the switch trials, a further 3s from the beginning of each trial was excluded to discard the initial easy phase of this task (e.g., 1, a, 2, b, 3, c). One power value for each condition was obtained by concatenating its data across trials and averaging across time points. For each pair of conditions (switch>count, count>rest), the percentage of signal change was computed as: [(power in condition 1/power in condition 2) – 1] * 100.

For each electrode, a permutation testing approach was used to statistically compare power change across each pair of conditions. For each electrode, the instantaneous power timeseries of all task trials from both conditions were concatenated serially to form a loop in the same order in which they were conducted. To close the loop, the end of the last trial was joined to the beginning of the first trial. All trial onset/offset markers were then shifted using the same jitter (randomly generated for each permutation), allowing them to "rotate" along the data loop. This rotation approach was used to generate surrogate power data while preserving trial lengths and the temporal correlations in the data. After the rotation, we computed the mean power (for each condition) and power ratio (across conditions) based on the new trial markers. Applying this rotation approach on the timeseries of the power rather than the raw data ensured that there were no artefacts in the form of sudden power changes at the points of trials concatenation. This process was repeated 100,000 times to create a surrogate distribution against which two-tailed statistical significance was calculated (percentile ranks 97.5 and 2.5) for each electrode.

To relate electrode locations with control-related regions identified by fMRI studies, a canonical resting-state fronto-parietal network (FPN) volumetric mask was used (Thomas Yeo et al., 2011). To match the original resolution of electrode localization using the grid method, the volumetric mask was resampled to 2 x 2 x 2 mm, then binarized to include any voxel with a non-zero probability. A volumetric approach was used rather than a surface-based approach because the presence of cortical lesions (i.e., the tumour) prevented accurate cortical surface extraction.

Table 1. Patient demographics

Patient	**Age**	**Sex**	**Tumour**	
			hemisphere	Main location
1	21-25	Male	Left	Frontal
2	21-25	Male	Left	Frontal
3	41-45	Female	Left	Frontal
4	26-30	Male	Left	Temporal
5	51-55	Female	Left	Frontal
6	21-25	Female	Right	Frontal
7	26-30	Male	Right	Frontal
8	36-40	Female	Right	Frontal
9	26-30	Male	Left	Frontal
10	31-35	Female	Left	Temporal
11	26-30	Female	Left	Temporal
12	56-60	Female	Left	Temporal
13	26-30	Male	Left	Frontal

Acknowledgments

The Royal Society provided financial support in the form of a Royal Society Dorothy Hodgkin Research Fellowship to YE (DH130100). Cambridge Commonwealth European and International Trust provided financial support in the form of a Yousef Jameel scholarship to MA. Guarantors of Brain provided financial support in the form of a Post-Doctoral Fellowship award to RRG. The National Institute for Health Research (NIHR, UK) provided financial support in the form of a Clinician Scientist Award 35 to SJP (ref: NIHR/CS/009/011). The Brain Tumour Charity provided financial support in the form of a grant award to MGH, TS and YE (ref: RG86218). J.D was funded by a Medical Research Council grant (SUAG/045.G101400). All the sponsors had no role in the design or conduct of this research. We thank Mallory Owen for help with administering and analyzing neuropsychological tests of the patients.

References

Assem M, Glasser MF, Van Essen DC, Duncan J. 2020. A Domain-General Cognitive Core Defined in Multimodally Parcellated Human Cortex. *Cereb Cortex* **30**:4361–4380. doi:10.1093/cercor/bhaa023

Badre D, Nee DE. 2018. Frontal Cortex and the Hierarchical Control of Behavior. *Trends Cogn Sci* **22**:170–188. doi:10.1016/j.tics.2017.11.005

Basilakos A, Smith KG, Fillmore P, Fridriksson J, Fedorenko E. 2018. Functional Characterization of the Human Speech Articulation Network. *Cereb Cortex* **28**:1816–1830. doi:10.1093/cercor/bhx100

Bouyer J., Montaron M., Rougeul A. 1981. Fast fronto-parietal rhythms during combined focused attentive behaviour and immobility in cat: cortical and thalamic localizations. *Electroencephalogr Clin Neurophysiol* **51**:244–252. doi:10.1016/0013-4694(81)90138-3

Buzsáki G, Wang X-J. 2012. Mechanisms of Gamma Oscillations. *Annu Rev Neurosci* **35**:203–225. doi:10.1146/annurev-neuro-062111-150444

Cole MW, Ito T, Braver TS. 2016. The Behavioral Relevance of Task Information in Human Prefrontal Cortex. *Cereb Cortex* **26**:2497–2505. doi:10.1093/cercor/bhv072

Corbetta M, Shulman GL. 2002. Control of goal-directed and stimulus-driven attention in the brain. *Nat Rev Neurosci* **3**:201–215. doi:10.1038/nrn755

Crone NE, Sinai A, Korzeniewska A. 2006. High-frequency gamma oscillations and human brain mapping with electrocorticographyProgress in Brain Research. pp. 275–295. doi:10.1016/S0079-6123(06)59019-3

Engell AD, Huettel S, McCarthy G. 2012. The fMRI BOLD signal tracks electrophysiological spectral perturbations, not event-related potentials. *Neuroimage* **59**:2600–2606. doi:10.1016/j.neuroimage.2011.08.079

Erez Y, Assem M, Coelho P, Romero-Garcia R, Owen M, McDonald A, Woodberry E, Morris RC, Price SJ, Suckling J, Duncan J, Hart MG, Santarius T. 2021. Intraoperative mapping of executive function using electrocorticography for patients with low-grade gliomas. *Acta Neurochir (Wien)* **163**:1299–1309. doi:10.1007/s00701-020-04646-6

Erez Y, Duncan J. 2015. Discrimination of Visual Categories Based on Behavioral Relevance in Widespread Regions of Frontoparietal Cortex. *J Neurosci* **35**:12383–12393. doi:10.1523/JNEUROSCI.1134-15.2015

Farahibozorg S-R, Henson RN, Hauk O. 2018. Adaptive cortical parcellations for source reconstructed EEG/MEG connectomes. *Neuroimage* **169**:23–45. doi:10.1016/j.neuroimage.2017.09.009

Fedorenko E, Duncan J, Kanwisher N. 2013. Broad domain generality in focal regions of frontal and parietal cortex. *Proc Natl Acad Sci* **110**:16616–16621. doi:10.1073/pnas.1315235110

Fellner M-C, Gollwitzer S, Rampp S, Kreiselmeyr G, Bush D, Diehl B, Axmacher N, Hamer H, Hanslmayr S. 2019. Spectral fingerprints or spectral tilt? Evidence for distinct oscillatory signatures of memory formation. *PLOS Biol* **17**:e3000403. doi:10.1371/journal.pbio.3000403

Fries P. 2001. Modulation of Oscillatory Neuronal Synchronization by Selective Visual Attention. *Science (80-)* **291**:1560–1563. doi:10.1126/science.1055465

Glasser MF, Coalson TS, Robinson EC, Hacker CD, Harwell J, Yacoub E, Ugurbil K, Andersson J, Beckmann CF, Jenkinson M, Smith SM, Van Essen DC. 2016. A multi-modal parcellation of human cerebral cortex. *Nature* **536**:171–178. doi:10.1038/nature18933

Gordon EM, Laumann TO, Adeyemo B, Huckins JF, Kelley WM, Petersen SE. 2016. Generation and Evaluation of a Cortical Area Parcellation from Resting-State Correlations. *Cereb Cortex* **26**:288–303. doi:10.1093/cercor/bhu239

Haller M, Case J, Crone NE, Chang EF, King-Stephens D, Laxer KD, Weber PB, Parvizi J, Knight RT, Shestyuk AY. 2018. Persistent neuronal activity in human prefrontal cortex links perception and action. *Nat Hum Behav* **2**:80–91. doi:10.1038/s41562-017-0267-2

Hart MG, Romero-Garcia R, Price SJ, Santarius T, Suckling J. 2020. Connections, Tracts, Fractals, and the Rest: A Working Guide to Network and Connectivity Studies in Neurosurgery. *World Neurosurg*. doi:10.1016/j.wneu.2020.03.116

Havas V, Gabarrós A, Rifa-ros X, Plans G. 2015. Brain & Language Electrical stimulation mapping of nouns and verbs in Broca ' s area **146**:53–63. doi:10.1016/j.bandl.2015.04.005

Helfrich RF, Knight RT. 2016. Oscillatory Dynamics of Prefrontal Cognitive Control. *Trends Cogn Sci* **20**:916–930. doi:10.1016/j.tics.2016.09.007

Hermes D, Miller KJ, Noordmans HJ, Vansteensel MJ, Ramsey NF. 2010. Automated electrocorticographic electrode localization on individually rendered brain surfaces. *J Neurosci Methods* **185**:293–298. doi:10.1016/j.jneumeth.2009.10.005

Hermes D, Miller KJ, Vansteensel MJ, Aarnoutse EJ, Leijten FSS, Ramsey NF. 2012a. Neurophysiologic correlates of fMRI in human motor cortex. *Hum Brain Mapp* **33**:1689–1699. doi:10.1002/hbm.21314

Hermes D, Siero JCW, Aarnoutse EJ, Leijten FSS, Petridou N, Ramsey NF. 2012b. Dissociation between Neuronal Activity in Sensorimotor Cortex and Hand Movement Revealed as a Function of Movement Rate. *J Neurosci* **32**:9736–9744.

doi:10.1523/JNEUROSCI.0357-12.2012

Howard MW. 2003. Gamma Oscillations Correlate with Working Memory Load in Humans. *Cereb Cortex* **13**:1369–1374. doi:10.1093/cercor/bhg084

Hugdahl K, Raichle ME, Mitra A, Specht K. 2015. On the existence of a generalized non-specific task-dependent network. *Front Hum Neurosci* **9**:430. doi:10.3389/fnhum.2015.00430

Jackson J, Rich AN, Williams MA, Woolgar A. 2016. Feature-selective Attention in Frontoparietal Cortex: Multivoxel Codes Adjust to Prioritize Task-relevant Information. *J Cogn Neurosci* **29**:310–321. doi:10.1162/jocn_a_01039

Jenkinson M, Beckmann CF, Behrens TEJ, Woolrich MW, Smith SM. 2012. FSL. *Neuroimage* **62**:782–790. doi:10.1016/j.neuroimage.2011.09.015

Lachaux J-P, Axmacher N, Mormann F, Halgren E, Crone NE. 2012. High-frequency neural activity and human cognition: Past, present and possible future of intracranial EEG research. *Prog Neurobiol* **98**:279–301. doi:10.1016/j.pneurobio.2012.06.008

Logothetis NK. 2008. What we can do and what we cannot do with fMRI. *Nature* **453**:869–878. doi:10.1038/nature06976

Logothetis NK, Pauls J, Augath M, Trinath T, Oeltermann A. 2001. Neurophysiological investigation of the basis of the fMRI signal. *Nature* **412**:150–157. doi:10.1038/35084005

Lundqvist M, Herman P, Lansner A. 2011. Theta and Gamma Power Increases and Alpha/Beta Power Decreases with Memory Load in an Attractor Network Model. *J Cogn Neurosci* **23**:3008–3020. doi:10.1162/jocn_a_00029

Mainy N, Kahane P, Minotti L, Hoffmann D, Bertrand O, Lachaux J-P. 2007. Neural correlates of consolidation in working memory. *Hum Brain Mapp* **28**:183–193. doi:10.1002/hbm.20264

Miller EK, Lundqvist M, Bastos AM. 2018. Working Memory 2.0. *Neuron* **100**:463–475. doi:10.1016/j.neuron.2018.09.023

Muhle-Karbe PS, De Baene W, Brass M. 2014. Do tasks matter in task switching? Dissociating domain-general from context-specific brain activity. *Neuroimage* **99**:332–341. doi:10.1016/j.neuroimage.2014.05.058

Mukamel R, Gelbard H, Arieli A, Hasson U, Fried I, Malach R. 2005. Coupling Between Neuronal Firing, Field Potentials, and fMRI in Human Auditory Cortex. *Science (80-)* **309**:951–954. doi:10.1126/science.1110913

Nir Y, Fisch L, Mukamel R, Gelbard-Sagiv H, Arieli A, Fried I, Malach R. 2007. Coupling between Neuronal Firing Rate, Gamma LFP, and BOLD fMRI Is Related to Interneuronal Correlations. *Curr Biol* **17**:1275–1285. doi:10.1016/j.cub.2007.06.066

Ojemann G, Ojemann J, Lettich E, Berger M. 1989. Cortical language localization in left,

dominant hemisphere. *J Neurosurg* **71**:316–326. doi:10.3171/jns.1989.71.3.0316

Podvalny E, Noy N, Harel M, Bickel S, Chechik G, Schroeder CE, Mehta AD, Tsodyks M, Malach R. 2015. A unifying principle underlying the extracellular field potential spectral responses in the human cortex. *J Neurophysiol* **114**:505–519. doi:10.1152/jn.00943.2014

Power JD, Cohen AL, Nelson SM, Wig GS, Barnes KA, Church JA, Vogel AC, Laumann TO, Miezin FM, Schlaggar BL, Petersen SE. 2011. Functional Network Organization of the Human Brain. *Neuron* **72**:665–678. doi:10.1016/j.neuron.2011.09.006

Ray S, Maunsell JHR. 2011. Different Origins of Gamma Rhythm and High-Gamma Activity in Macaque Visual Cortex. *PLoS Biol* **9**:e1000610. doi:10.1371/journal.pbio.1000610

Ray S, Niebur E, Hsiao SS, Sinai A, Crone NE. 2008. High-frequency gamma activity (80–150Hz) is increased in human cortex during selective attention. *Clin Neurophysiol* **119**:116–133. doi:10.1016/j.clinph.2007.09.136

Shashidhara S, Mitchell DJ, Erez Y, Duncan J. 2019. Progressive Recruitment of the Frontoparietal Multiple-demand System with Increased Task Complexity, Time Pressure, and Reward. *J Cogn Neurosci* **31**:1617–1630. doi:10.1162/jocn_a_01440

Shashidhara S, Spronkers FS, Erez Y. 2020. Individual-subject Functional Localization Increases Univariate Activation but Not Multivariate Pattern Discriminability in the "Multiple-demand" Frontoparietal Network. *J Cogn Neurosci* **32**:1348–1368. doi:10.1162/jocn_a_01554

Siero JC, Hermes D, Hoogduin H, Luijten PR, Petridou N, Ramsey NF. 2013. BOLD consistently matches electrophysiology in human sensorimotor cortex at increasing movement rates: a combined 7T fMRI and ECoG study on neurovascular coupling. *J Cereb Blood Flow Metab* **33**:1448–1456. doi:10.1038/jcbfm.2013.97

Stolk A, Griffin S, van der Meij R, Dewar C, Saez I, Lin JJ, Piantoni G, Schoffelen J-M, Knight RT, Oostenveld R. 2018. Integrated analysis of anatomical and electrophysiological human intracranial data. *Nat Protoc* **13**:1699–1723. doi:10.1038/s41596-018-0009-6

Szczepanski SM, Crone NE, Kuperman RA, Auguste KI, Parvizi J, Knight RT. 2014. Dynamic Changes in Phase-Amplitude Coupling Facilitate Spatial Attention Control in Fronto-Parietal Cortex. *PLoS Biol* **12**:e1001936. doi:10.1371/journal.pbio.1001936

Thomas Yeo BT, Krienen FM, Sepulcre J, Sabuncu MR, Lashkari D, Hollinshead M, Roffman JL, Smoller JW, Zöllei L, Polimeni JR, Fischl B, Liu H, Buckner RL. 2011. The organization of the human cerebral cortex estimated by intrinsic functional connectivity. *J Neurophysiol* **106**:1125–1165. doi:10.1152/jn.00338.2011

Voytek B, Kayser AS, Badre D, Fegen D, Chang EF, Crone NE, Parvizi J, Knight RT,

D'Esposito M. 2015. Oscillatory dynamics coordinating human frontal networks in support of goal maintenance. *Nat Neurosci* **18**:1318–1324. doi:10.1038/nn.4071

Yeo BTT, Krienen FM, Eickhoff SB, Yaakub SN, Fox PT, Buckner RL, Asplund CL, Chee MWL. 2015. Functional Specialization and Flexibility in Human Association Cortex. *Cereb Cortex* **25**:3654–3672. doi:10.1093/cercor/bhu217

Yeo BTT, Krienen FM, Sepulcre J, Sabuncu MR, Lashkari D, Hollinshead M, Roffman JL, Smoller JW, Zöllei L, Polimeni JR, Fischl B, Liu H, Buckner RL. 2011. The organization of the human cerebral cortex estimated by intrinsic functional connectivity. *J Neurophysiol* **106**:1125–1165. doi:10.1152/jn.00338.2011